

# Robust Topological Order in Fermionic $\mathbb{Z}_2$ Gauge Theories: From Aharonov-Bohm Instability to Soliton-Induced Deconfinement


Daniel González-Cuadra<sup>1,\*</sup>, Luca Tagliacozzo,<sup>2</sup> Maciej Lewenstein,<sup>1,3</sup> and Alejandro Bermudez<sup>4</sup>

<sup>1</sup>*ICFO—Institut de Ciències Fotòniques, The Barcelona Institute of Science and Technology, Avinguda Carl Friedrich Gauss 3, 08860 Castelldefels (Barcelona), Spain*

<sup>2</sup>*Departament de Física Quàntica i Astrofísica and Institut de Ciències del Cosmos (ICCUB), Universitat de Barcelona, Martí i Franquès 1, 08028 Barcelona, Spain*

<sup>3</sup>*ICREA, Lluís Companys 23, 08010 Barcelona, Spain*

<sup>4</sup>*Departamento de Física Teórica, Universidad Complutense, 28040 Madrid, Spain*

 (Received 3 March 2020; revised 28 May 2020; accepted 14 August 2020; published 9 October 2020)

Topologically ordered phases of matter, although stable against local perturbations, are usually restricted to relatively small regions in phase diagrams. Thus, their preparation requires a precise fine-tuning of the system's parameters, a very challenging task in most experimental setups. In this work, we investigate a model of spinless fermions interacting with dynamical  $\mathbb{Z}_2$  gauge fields on a cross-linked ladder and show evidence of topological order throughout the full parameter space. In particular, we show how a magnetic flux is spontaneously generated through the ladder due to an Aharonov-Bohm instability, giving rise to topological order even in the absence of a plaquette term. Moreover, the latter coexists here with a symmetry-protected topological phase in the matter sector, which displays fractionalized gauge-matter edge states and intertwines with it by a flux-threading phenomenon. Finally, we unveil the robustness of these features through a gauge frustration mechanism, akin to geometric frustration in spin liquids, allowing topological order to survive to arbitrarily large quantum fluctuations. In particular, we show how, at finite chemical potential, topological solitons are created in the gauge field configuration, which bound to fermions and form  $\mathbb{Z}_2$  deconfined quasiparticles. The simplicity of the model makes it an ideal candidate for 2D gauge theory phenomena, as well as exotic topological effects, to be investigated using cold-atom quantum simulators.

DOI: [10.1103/PhysRevX.10.041007](https://doi.org/10.1103/PhysRevX.10.041007)

Subject Areas: Atomic and Molecular Physics,  
Condensed Matter Physics,  
Particles and Fields

## I. INTRODUCTION

Understanding quantum many-body systems is generally a difficult problem, as their complexity increases exponentially with the number of constituents. From this large complexity, exotic collective phenomena may arise, as occurs for the so-called spin liquids. These phases of matter evade spontaneous symmetry breaking, and thus long-range order [1], down to the lowest possible temperatures [2–4]. In spite of this, spin liquids can be characterized by a different notion of order: topological order [5]. Systems with topological order have degenerate ground states, the number of which depends on the underlying topology. Each ground state is a strongly correlated state, as

witnessed by the multipartite long-range entanglement among the constituents [6,7]. Besides, the ground-state manifold is separated from the rest of the spectrum by a finite energy gap, and more importantly, only nonlocal perturbations can act nontrivially within it. It is thus a natural subspace to encode quantum information and a promising route for fault-tolerant quantum computers [8,9].

Unfortunately, topological order is very elusive and tends to be fragile, as witnessed by the few materials where it has been observed, in many cases requiring extremely low temperatures and very high purity in the samples [10,11]. Here, we identify a promising route to prepare robust topologically ordered states in cold-atom systems using gauge invariance.

Gauge theories—used to describe strong, weak, and electromagnetic interactions [12]—have local symmetries that cannot be broken spontaneously [13], thus evading the standard form of ordering. For this reason [14], emergent gauge theories also play an important role in long-wavelength descriptions of nonstandard phases of matter, such as high- $T_c$  superconductors [15] and frustrated

\*daniel.gonzalez@icfo.eu

Published by the American Physical Society under the terms of the [Creative Commons Attribution 4.0 International license](https://creativecommons.org/licenses/by/4.0/). Further distribution of this work must maintain attribution to the author(s) and the published article's title, journal citation, and DOI.

magnets [16]. Formally, gauge theories can be described through Hamiltonians that commute with an extensive number of local symmetry operators forming a group, the gauge group [17].

Pure gauge theories describe the physics of gauge bosons and the generalization of photons to arbitrary gauge groups [18], and host different phases that can be characterized by the potential for the bosons to mediate between test charges [12,19]. In a deconfined phase, particles generated in pairs of opposite charge can be separated arbitrarily far away with a finite energy cost. Conversely, there can also exist confined phases where this potential energy increases linearly with the distance. The simplest gauge theory on the lattice [20], the so-called  $\mathbb{Z}_2$  or Ising gauge theory (IGT), already gives rise to a confined-deconfined phase transition without spontaneous symmetry breaking [21]. We note that the very nature of this deconfined phase is the key underlying topological order in Kitaev's toric code [8], a spin-liquid phase allowing for topological quantum error correction and fault-tolerant quantum computing [22]. It is thus important, both from fundamental and applied perspectives, to study the fate of the IGT deconfined phase and, more generally, its full phase diagram as perturbations are introduced [8,23–26]. Understanding such phase diagrams when the gauge fields interact with matter fields, either bosonic or fermionic, is generally a very hard problem with longstanding open questions [12]. In the simplest case, the topologically ordered deconfined phase of the IGT coupled to dynamical  $\mathbb{Z}_2$  matter can be understood through the toric code perturbed by both parallel and transverse fields [8,27–29]. While the corresponding phase diagram has been known since the late 1970s [27], exchanging  $\mathbb{Z}_2$  for fermionic matter leads to a much richer scenario, which is only in the initial stages of exploration [30–34].

These connections have fuelled a multidisciplinary effort towards not only improving our understanding of these lattice gauge theories (LGTs) but also realizing them experimentally, either in natural or in synthetic quantum materials, such as cold atoms in optical lattices [35]. These are systems where atoms are very dilute and, thus, primarily interact by  $s$ -wave scattering. Trapping the atoms with an optical lattice allows us to reach the strongly interacting regime, but the interactions are still limited to being on site [36]. This fact constitutes a major hurdle when trying to realize lattice gauge theories with ultracold atoms [37–40], as they require interactions between all of the atoms connected through elementary loops of the lattice (i.e., plaquettes) [41–49]. Aside from this point, the implementation of the tunneling of matter dressed by the gauge fields is also far from trivial. Floquet engineering in strongly interacting gases [50–52] and spin-changing collisions in atomic mixtures [53–56] have identified neat directions towards this goal, which are particularly promising in light of recent experiments [57–60]. Since the realization of

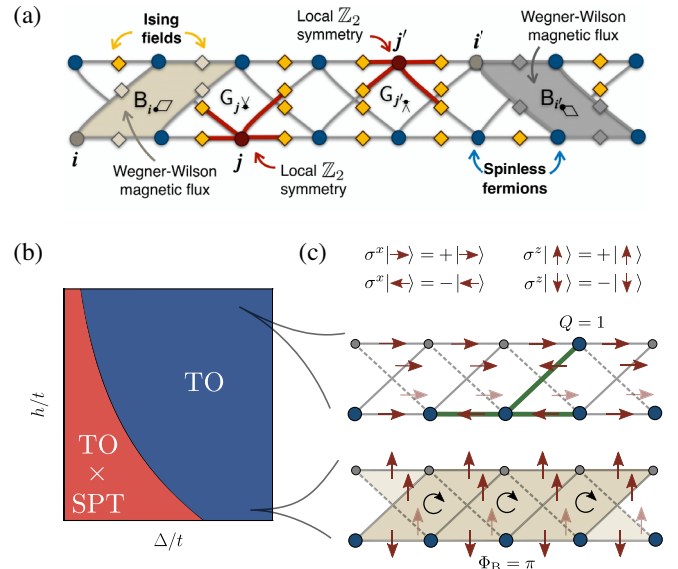


FIG. 1. Creutz-Ising ladder. (a) Spinless fermions, which reside on the sites of a two-leg ladder (filled circles) and can tunnel along and across the legs forming a cross-linked pattern. These tunnelings are minimally dressed by Ising spin-1/2 fields, which sit on the corresponding links (filled rhombi). We represent the Wegner-Wilson fluxes across the two minimal plaquettes (tilted trapezoids in grey) and the generators of the local  $\mathbb{Z}_2$  symmetries (red graphs). (b) Sketch of the phase diagram at half filling in terms of the electric field  $h$  and the imbalance  $\Delta$ . We find two phases, both with topological order (TO). In one case, the latter coexists with a SPT in the matter sector. (c) For  $\Delta \gg t$ , the fermions populate the lower leg of the ladder. At  $h \ll t$ , the Ising fields rearrange to spontaneously generate a  $\pi$  flux per plaquette through an Aharonov-Bohm instability, giving rise to TO. For  $h \gg t$ , the latter survives due to a gauge frustration mechanism. Fermions delocalize by forming bound quasiparticles with topological defects created in an otherwise dimerized electric-field background.

plaquette terms is currently the major experimental bottleneck to simulate gauge theories beyond 1D, a timely question would be as follows: Is it possible to find characteristic features, such as deconfinement and topological order, in lattice gauge theories without plaquette terms?

In this work, we show that it is indeed possible to find such features. By studying a cross-linked lattice connectivity (see Fig. 1), we identify a new avenue for the interplay of local symmetries and topology in LGTs, as an Aharonov-Bohm instability can induce a magnetic flux in the absence of plaquette terms, giving rise to topological order that, in this case, coexists with a symmetry-protected topological (SPT) phase [61]. The crucial role that gauge symmetry plays in the topological properties of the system extends to large quantum fluctuations through a frustration mechanism, allowing deconfinement to survive for the whole phase diagram.

The paper is organized as follows. In Sec. II, we introduce the Creutz-Ising ladder, a quasi-1D  $\mathbb{Z}_2$  LGT where the Ising fields are coupled to spinless fermions hopping in a cross-linked ladder, and we summarize our main findings. In Sec. III, we describe the Aharonov-Bohm instability and the emergence of a magnetic flux, which gives rise to a SPT phase. We study this phenomenon in the presence of quantum fluctuations of the gauge fields and provide a full discussion of the phase diagram. In Sec. IV, we demonstrate that the cross-linked ladder can be understood as the thin-cylinder limit of a 2D LGT, providing a practical scenario where the ground-state degeneracy is related to the topology of the underlying manifold. In Sec. V, we explore the mechanism of fermionic deconfinement mediated by topological solitons, which can be neatly understood in the limit of large quantum fluctuations through a gauge frustration effect. Finally, we present our conclusions and outlook in Sec. VI.

## II. CREUTZ-ISING LADDER

### A. Model

The Creutz-Ising (CI) ladder, which describes spinless fermions on a cross-linked ladder [62], is a lattice model hosting a SPT phase. The tunneling of fermions is dressed by a static magnetic field that pierces the ladder, which is described by a gauge-invariant flux that pierces the elementary plaquettes. For a static  $\pi$  flux, the ground state of this model may correspond to either the BDI or the AIII class of topological insulators [63], a free-fermion insulating SPT phase. Interestingly, the physics of cross-linked ladders has already been explored in experiments of ultracold atoms by exploiting Floquet engineering in two-orbital optical lattices [64,65]. To go beyond this free-fermion scenario, a natural possibility is to include Hubbard-type interactions [66], which leads to correlated SPT phases with interesting connections to relativistic quantum field theories of self-interacting fermions [67,68].

We hereby follow a different, and yet unexplored, route: We upgrade the background magnetic fields to a  $\mathbb{Z}_2$  LGT by introducing Ising fields on the links [see Fig. 1(a)]. This IGT is described by the following Hamiltonian:

$$H_{\text{CI}}(t, \Delta, h) = \sum_i \sum_{(ij)} (-t c_i^\dagger \sigma_{(ij)}^z c_j - h \sigma_{(ij)}^x) + \frac{\Delta}{2} \sum_i s_i c_i^\dagger c_i, \quad (1)$$

where  $c_i^\dagger$  ( $c_i$ ) creates (annihilates) a fermion at site  $i = (i_1, i_2)$ . Here,  $i_2 \in \mathbb{Z}_2 = \{0, 1\}$  labels the lower and upper legs of the ladder, and  $i_1 \in \mathbb{Z}_{N_s} = \{0, \dots, N_s - 1\}$  labels the sites of each of these legs. At the horizontal or diagonal links  $(i, j)$  adjacent to  $i$ , we introduce the Pauli matrices  $\sigma_{(ij)}^z, \sigma_{(ij)}^x$  as the corresponding Ising link operators. The first term of Eq. (1) describes the tunneling of

fermions dressed by the Ising gauge fields, which has tunneling strength  $t$ . The second term introduces an electric transverse field of strength  $h$ . Finally, the third term describes an energy imbalance of magnitude  $\Delta$  for the fermions sitting on the upper leg  $s_i = +1$  or lower leg  $s_i = -1$ .

The above Hamiltonian (1) displays a local  $\mathbb{Z}_2$  symmetry  $[H_{\text{CI}}, \mathbf{G}_i] = 0$ ,  $\forall i \in \mathbb{Z}_{N_s} \times \mathbb{Z}_2$ , with the generators

$$G_{i\blacktriangledown} = (-1)^{c_i^\dagger c_i} \prod_{(i,j) \in i\blacktriangledown} \sigma_{(i,j)}^x, \quad G_{i\blacktriangleright} = (-1)^{c_i^\dagger c_i} \prod_{(i,j) \in i\blacktriangleright} \sigma_{(i,j)}^x, \quad (2)$$

displayed in Fig. 1(a). In addition, in this figure we also depict the smallest Wegner-Wilson loops, corresponding to gauge-invariant magnetic fields across two types of trapezia,

$$B_{i\blacktriangledown} = \prod_{(i,j) \in i\blacktriangledown} \sigma_{(i,j)}^z, \quad B_{i\blacktriangleright} = \prod_{(i,j) \in i\blacktriangleright} \sigma_{(i,j)}^z, \quad (3)$$

with corresponding magnetic fluxes

$$\Phi_B^{i\blacktriangledown} = \arccos(\langle B_{i\blacktriangledown} \rangle), \quad \Phi_B^{i\blacktriangleright} = \arccos(\langle B_{i\blacktriangleright} \rangle). \quad (4)$$

The magnetic flux that threads a plaquette corresponds to the phase accumulated by a particle that encircles that plaquette. Using this picture, we can write down the spin operators present in the gauge-invariant tunneling terms of Eq. (1) as dynamical  $\mathbb{Z}_2$  Peierls phases,  $\sigma_{(ij)}^z = e^{i\varphi_{(ij)}}$ , where  $\varphi_{(ij)}$  has eigenvalues 0 and  $\pi$ .

We note that, in the standard formulation of IGTs [69], one also introduces an additional magnetic-field term

$$\tilde{H}_{\text{CI}}(t, \Delta, h, J) = H_{\text{CI}}(t, \Delta, h) - J \sum_i (B_{i\blacktriangledown} + B_{i\blacktriangleright}), \quad (5)$$

such that the magnetic plaquette coupling  $J$  competes with the electric transverse field  $h$ . In the  $(2+1)$  pure IGT, this competition leads to a quantum phase transition between deconfined  $h/J < h/J|_c$  and confined  $h/J > h/J|_c$  phases [21]. These phases are not characterized by a local order parameter but instead display Wegner-Wilson loops that scale either with the perimeter ( $h/J < h/J|_c$ ) or with the encircled area ( $h/J > h/J|_c$ ) of a closed loop, i.e., perimeter or area law.

The  $\mathbb{Z}_2$  symmetry generators (2) can be used to define different charge sectors of the Hilbert space, as the eigenstates of the Hamiltonian  $|\psi\rangle$  must also fulfill

$$G_i |\psi\rangle = (-1)^{q_i} |\psi\rangle, \quad (6)$$

where  $q_i \in \{0, 1\}$  are the so-called static  $\mathbb{Z}_2$  charges. Typically, one considers the vacuum or even sector

$\{q_i\} = \{0, 0, \dots, 0\}$ , introducing a few static charges on top of it. For instance,  $\{q_i\} = \{\delta_{i,(i_0,0)}, \delta_{i,(i_0+L,0)}\}$  describes a pair of static  $\mathbb{Z}_2$  charges separated by a distance  $L$ . In the  $(2+1)$  pure IGT [12], these test charges are subjected to a potential  $V(L) = E_{\text{gs}}(L) - E_{\text{gs}}(0)$  that either remains constant in the deconfined phase  $V(L) \propto V_0$  or increases with the distance in the confined phase  $V(L) \propto L$ . We note that  $(2+1)$  is the lower critical dimension since the  $(1+1)$  IGT can only display an area law [12], solely hosting a confined phase. In the presence of fermionic matter, rather than through the aforementioned area law, the  $(1+1)$  confined phase can be characterized through the appearance of chargeless bound dimers [70].

In this work, we argue that fermionic  $\mathbb{Z}_2$  gauge theories in quasi-1D geometries, such as the ladder structure of Fig. 1, lead to a much richer playground in comparison to the strict 1D limit [Fig. 1(b)]. Let us summarize our main findings.

### B. Summary of our results

In the pure gauge sector, which is obtained from Eq. (5) by setting  $t = \Delta = 0$ , we show that  $\tilde{H}_{\text{CI}}(0, 0, h, J)$  still hosts a quantum phase transition at a critical  $h/J|_c$ , separating confined and deconfined phases. We characterize this phase transition quantitatively using matrix-product-state (MPS) numerical simulations [71], which allow us to extract the critical behavior of the Ising magnetic fluxes and their susceptibilities. We note that the ladder geometry plays a key role to go beyond the  $(1+1)$  lower critical dimension [12]. By switching on the coupling to the dynamical fermions, we show that the aforementioned Aharonov-Bohm instability takes place and results in an emerging  $\pi$ -flux deconfined phase even in the absence of the magnetic plaquette term [Fig. 1(c)], namely, setting  $J = 0$  in the Creutz-Ising Hamiltonian  $\tilde{H}_{\text{CI}}(t, \Delta, h, 0)$ . We explicitly demonstrate the presence of topological order by calculating the topological entanglement entropy associated with the ground-state wave function [72,73]. As opposed to pure gauge theory, we show how the accompanying deconfinement survives in the limit of arbitrary quantum fluctuations set by large transverse fields  $h$  [Fig. 1(c)]. Here, single  $\mathbb{Z}_2$  charges can be localized within topological solitons that interpolate between two different symmetry-breaking orders. We believe that this is a generic feature of IGTs in the particular charge sector considered in this work. To the best of our knowledge, this study provides the first quantitative analysis of such a deconfinement mechanism.

Moreover, as a result of the cross-linked geometry, we also show that the matter sector may lie in a SPT phase characterized by a nonzero topological invariant. From the perspective of the fermions, the corresponding topological edge states can be understood as domain-wall fermions [74–76] with the novelty that, instead of requiring fine-tuning to incorporate chiral symmetry on the lattice, they

are spontaneously generated by the Ising-matter coupling. The fact that a plaquette term  $J \neq 0$  is not required to host this exotic behavior is particularly interesting in light of current developments in cold-atom quantum simulations. Interestingly, the interplay between geometry and gauge-invariant interactions allows us to obtain a topological phase for gauge fields without introducing four-body plaquette terms, enormously simplifying the experimental implementation. This point is important since the main building blocks of the model have already been realized in cold-atom experiments [57]. Therefore, future quantum simulations of this fermionic IGT will be capable of testing the nontrivial equilibrium properties described in this work.

### III. AHARONOV-BOHM INSTABILITY

We start by exploring the limit of zero electric-field strength  $h = 0$ . In the following, and unless stated otherwise, we fix  $J = 0$ . Here, the Ising fields have vanishing quantum fluctuations, and the fermions tunnel in a classical  $\mathbb{Z}_2$  background  $|\{\sigma_{(ij)}\}\rangle$ , where  $\sigma_{(ij)} = \pm 1$  are the eigenvalues of the  $\sigma^z$  link operator. In this limit, there are only two translationally invariant ground states corresponding to the 0- or  $\pi$ -flux configurations, namely,  $\langle \mathbb{B}_{i\leftarrow j} \rangle = \langle \mathbb{B}_{i\leftarrow i} \rangle = \pm 1$ . The fermions minimize their energy in these backgrounds by partially filling the corresponding energy bands  $\varepsilon_{\pm}^0(k)$  or  $\varepsilon_{\pm}^{\pi}(k)$ .

For vanishing imbalance  $\Delta = 0$ , and considering periodic boundary conditions, these band structures read

$$\varepsilon_{\pm}^0(k) = -2t \cos k \pm 2t |\cos k|, \quad \varepsilon_{\pm}^{\pi}(k) = \pm 2t, \quad (7)$$

where  $k \in [-\pi, \pi)$ . As depicted in Fig. 2(a), for magnetic flux  $\Phi_{\text{B}} = 0$ , the half-filled ground state corresponds to a gapless state. Conversely, for  $\Phi_{\text{B}} = \pi$  flux [Fig. 2(b)], the band structure consists of two flat bands, such that the half-filled ground state is a single gapped state with a fully occupied lowest band. By direct inspection of Fig. 2, it is apparent that the  $\pi$ -flux case is energetically favorable, which is indeed the case, as one finds that  $E_{\text{gs}}^{\pi} = -2tN_s < -(4t/\pi)N_s = E_{\text{gs}}^0$ . We recall the Peierls instability in 1D metals [77], where the underlying lattice adopts a dimerized configuration and a gap is opened in the metallic band; here, it is the Ising fields that adopt a  $\pi$ -flux configuration leading to a gap opening in the fermionic sector. This spontaneous generation of a  $\pi$  flux is in accordance with Lieb's result for bipartite lattices [78], but, in contrast to the square lattice [30,31,33], it does not lead to a semimetallic phase with emergent Dirac fermions [79]. In this case, it is an insulator with complete band flattening caused by destructive Aharonov-Bohm interference at  $\Phi_{\text{B}} = \pi$  [80], which can result in many-body localization [81]. Because of the remarkable similarities with the Peierls effect, we call this effect the Aharonov-Bohm instability.

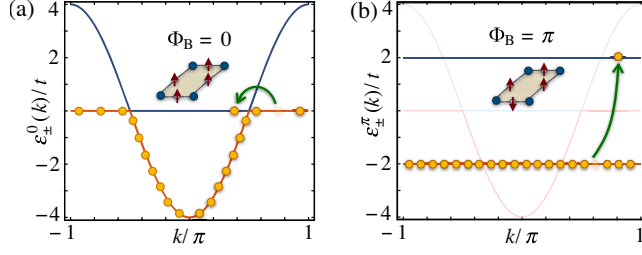


FIG. 2. Aharonov-Bohm instability. Band structure of the Creutz-Ising gauge theory for  $J = h = \Delta = 0$ , and the corresponding filling of the fermionic sector. The green arrows depict the lowest-energy particle-hole excitations of the half-filled ladder. (a) For an Ising background with a vanishing flux  $\Phi_B = 0$ , the ground state corresponds to a gapless state with macroscopic degeneracy. (b) For  $\Phi_B = \pi$ , there is destructive Aharonov-Bohm interference that opens a gap, forming two flat bands and lowering the ground-state energy (the semitransparent lines serve to compare to the  $\Phi_B = 0$  case).

This flux instability is actually generic for any imbalance  $\Delta > 0$ , in spite of the fact that the bands gain curvature. In this case, the corresponding ground-state energies are

$$\begin{aligned} E_{\text{gs}}^0 &= -\frac{4t}{\pi} ((1 + \xi^2)^{1/2} \mathbf{E}(\theta_0)) N_s, \\ E_{\text{gs}}^\pi &= -\frac{2t}{\pi} (|1 + \xi| \mathbf{E}(\theta_\pi) + |1 - \xi| \mathbf{E}(\tilde{\theta}_\pi)) N_s, \end{aligned} \quad (8)$$

where we have introduced the parameters  $\xi = \Delta/4t$ ,  $\theta_0 = 1/(1 + \xi^2)$ ,  $\theta_\pi = 4\xi/(1 + \xi)^2$ , and  $\tilde{\theta}_\pi = -4\xi/(1 - \xi)^2$ . Additionally, we have used the complete elliptic integral of the second kind,  $\mathbf{E}(x) = \int_0^{\pi/2} d\alpha (1 - x \sin^2 \alpha)^{1/2}$ . Once again, one can readily confirm that  $E_{\text{gs}}^\pi < E_{\text{gs}}^0$ , such that it is energetically favorable for the ground state to lie in the  $\pi$ -flux phase, which is generally gapped except for  $\xi = 1$ , namely,  $\Delta = 4t$ .

### A. Emerging Wilson fermions and SPT phases

By exploring the imbalanced case at long wavelengths, we can understand the insulating  $\pi$ -flux phase from a different perspective. Rather than the massless Dirac fermions that emerge in the square-lattice  $\pi$ -flux phase [30,31,33], we get the following long-wavelength dispersion around  $k_\pm = \pm\pi/2$ ,

$$\varepsilon_\pm^\pi(k_\pm + p) \approx \pm \sqrt{(m_\pm c^2)^2 + (cp)^2}, \quad m_\pm = (\xi \pm 1)/2t, \quad (9)$$

where  $c = 2t$  is the propagation speed and  $m_\pm$  are two mass parameters. Except for  $\xi = 1$ , we get two massive relativistic fermions characterized by a different mass, which are known as Wilson fermions in a LGT context [82].

The fact that the Wilson masses are different,  $m_+ \neq m_-$ , turns out to be crucial in connection to the spontaneous generation of a SPT phase. The Chern-Simons form  $\mathbf{Q}_1^\pi = \frac{i}{2\pi} \langle \varepsilon_\pm^\pi(k) | \partial_k | \varepsilon_\pm^\pi(k) \rangle dk$  [83], equivalent to the Zak phase in 1D [84], leads to a Chern-Simons invariant  $\mathcal{I}$  after integrating over all occupied quasimomenta,

$$\mathcal{I}_1^\pi = \int_{-\pi}^{\pi} \mathbf{Q}_1^\pi = \frac{1}{4} (\text{sgn}(m_+) - \text{sgn}(m_-)). \quad (10)$$

One can define a gauge-invariant Wilson loop  $\mathbf{W}_1^\pi = e^{i2\pi\mathcal{I}_1^\pi}$  that detects the nontrivial topology when  $\mathbf{W}_1^\pi = -1$ . The loop takes this value when the pair of Wilson fermions have masses with opposite signs. Accordingly, if  $|\xi| < 1$  (i.e.,  $-4t < \Delta < 4t$ ), the topological Wilson loop is nontrivial  $\mathbf{W}_1^\pi = -1$ , and the emerging  $\pi$ -flux phase is an insulating SPT phase.

This result draws a further analogy between the Peierls and Aharonov-Bohm instabilities. In the former, when the instability is triggered by an electron-lattice coupling that modulates the tunneling [85–87], one of the dimerization patterns of the lattice leads to a nonzero topological invariant and a SPT phase [88]. In our case, there is no dimerization due to SSB since the local  $\mathbb{Z}_2$  symmetry cannot be spontaneously broken. However, there are two gauge-invariant fluxes at  $h = 0$ , and only the  $\pi$ -flux configuration leads to a nonzero topological invariant when  $|\Delta| < 4t$ . We can thus conclude that, as a consequence of the Aharonov-Bohm instability, the fermions intertwine with the Ising fields in such a way that a gap is opened in the fermion sector with nontrivial topology.

### B. Gauge-matter edge states and fractionalization

So far, our discussion has revolved around the zero electric-field limit  $h = 0$ , and we have assumed periodic boundary conditions. From now on, we abandon this limit and explore the effect of quantum fluctuations in open Creutz-Ising ladders (i.e., Dirichlet or hard-wall boundary conditions). Because of the bulk-boundary correspondence, when the bulk of the spontaneously generated  $\pi$ -flux phase is characterized by a nonzero topological invariant (10), one expects that edge states will appear at the boundaries of the ladder. In the context of LGTs, these states are lower-dimensional domain-wall fermions [74] with the key difference that, in our case, they are generated via the Aharonov-Bohm instability.

In Fig. 3, we show the real-space configuration of both matter and Ising fields. We use a MPS-based algorithm [89] of the density-matrix renormalization group (DMRG) [90], setting the bond dimension to  $D = 200$  for a ladder of leg length  $N_s = 20$  at half-filling, and introduce quantum fluctuations through  $h = 0.1t$ . In these figures, we display the Ising flux

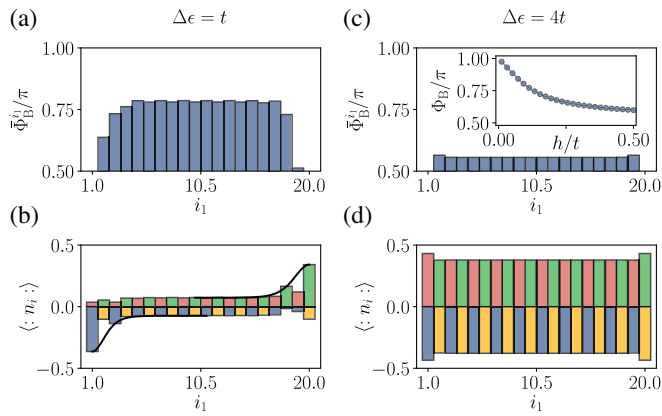


FIG. 3. Gauge-matter edge states. (a) Average Ising flux  $\bar{\Phi}_B^{i_1}$  in the ground state of the Creutz-Ising ladder for  $\Delta = t$  and  $h = 0.1t$ , for a ladder of length  $N_s = 20$  filled with  $N = 20$  particles. Because of the quantum fluctuations, the bulk flux gets lowered,  $\bar{\Phi}_B^{\text{bulk}} < \pi$ . (b) Fermionic occupation  $\langle :n_i: \rangle$  showing boundary peaks that can be identified with the topologically protected edge modes. We use red and green to represent odd and even sites, respectively, of the lower leg, and blue and yellow for the upper one. The solid black lines are obtained by fitting the latter to Eq. (13), showing that the excess and defect of the charge are due to the presence of edge states at zero energy. In panels (c) and (d), we can observe how, for a higher value of the imbalance ( $\Delta = 4t$ ), the edge states disappear. The inset shows the flux in an infinite ladder as a function of  $h/t$  for  $\Delta = 0.1t$ .

$$\bar{\Phi}_B^{i_1} = \frac{\Phi_B^{i_1 \blacktriangleleft} + \Phi_B^{i_1 \blacktriangleright}}{2} \quad (11)$$

averaged over the two trapezoidal plaquettes, and the normal-ordered fermionic occupation

$$\langle :n_i: \rangle = \langle c_i^\dagger c_i \rangle - \rho, \quad (12)$$

where  $\rho = 1/2$  at half-filling. As shown in Figs. 3(a) and 3(c), because of the quantum fluctuations, the Ising flux is no longer fixed at  $\pi$ . As the transverse field increases,  $\bar{\Phi}_B \rightarrow \pi/2$ , which amounts to an electric-field-dominated phase with a vanishing expectation value of the magnetic plaquettes  $\langle B_{i\blacktriangleleft} \rangle = \langle B_{i\blacktriangleright} \rangle = 0$ . In the inset, we show how the flux  $\Phi_B$  changes with  $h$  in an infinite ladder, where the ground state is obtained using the iDMRG algorithm with  $D = 200$  [89]. This change is continuous from  $h = 0$ , suggesting that the flux-dominated phase found in the absence of quantum fluctuations with  $\Phi_B = \pi$  extends to finite values of  $h$ . In the next section, we argue that this flux-dominated phase actually extends to the whole phase diagram, as in the case of  $h = 0$ .

In Fig. 3(b), we show that the corresponding fermion distribution is not translationally invariant but displays an excess or deficit of charge around the boundaries of the ladder. This real-space distribution is consistent with the existence of two topological edge states in the SPT phase,

one of them being filled while the other one remains empty at half-filling. We note that, in analogy with the phenomenon of charge fractionalization put forth by Jackiw and Rebbi [91], when these zero modes are occupied or empty, an excess or deficit of  $1/2$  fermion is formed around the boundaries. This fractionalization can be readily observed in Fig. 3(b), where we also show that the excess or deficit of charge with respect to the bulk density on each leg of the ladder  $\rho_{i_2}$  follows

$$\langle n_{(j,i_2)} \rangle - \rho_{i_2} = \pm \frac{1}{4\xi_\ell} \text{sech}^2\left(\frac{j - j_p}{\xi_\ell}\right). \quad (13)$$

Here,  $j = 2i_1$  (respectively,  $j = 2i_1 - 1$ ) is the sublattice index for the lower (respectively, upper) leg of the ladder, with  $j_p = L$  (respectively,  $j_p = 0$ ), and  $\xi_\ell$  is the localization length of the corresponding edge state. This behavior is a universal feature of zero modes in relativistic quantum field theories and condensed-matter models [92], and we show that it also holds for LGTs. In Fig. 3(b), we observe how the edge states disappear for higher values of the imbalance  $\Delta$ , signaling a transition towards a trivial phase.

The presence of edge states points towards the robustness of the SPT flux-dominated phase described in the previous section, which thus persists as one introduces nonzero quantum fluctuations. Therefore, the SPT phase should extend to a larger region in parameter space. Let us also highlight that, by looking at the enlarged fluctuations of the Ising flux close to the boundaries [Fig. 3(a)], one realizes that the edge states are indeed composite objects, where both the matter and gauge degrees of freedom are intertwined. We will unveil a very interesting consequence of this intertwining below.

### C. Topological phase transitions

We explore the extent of this SPT phase in parameter space ( $\Delta/t, h/t$ ). The topological invariant (10) is related to the Berry phase  $\gamma$  acquired by the ground state  $|E_{\text{gs}}(\theta)\rangle$  along an adiabatic Hamiltonian cycle  $\mathbf{H}(\theta) = \mathbf{H}(\theta + 2\pi)$  [93], namely,

$$\gamma = i \int_0^{2\pi} d\theta \langle E_{\text{gs}}(\theta) | \partial_\theta | E_{\text{gs}}(\theta) \rangle. \quad (14)$$

For noninteracting fermions in a classical  $\mathbb{Z}_2$  background, one can use quasimomentum as the adiabatic parameter  $\theta = k$ , such that  $\gamma = 2\pi \mathcal{I}_1^T$  (10). However, as the electric field is switched on, the Ising fields fluctuate quantum-mechanically mediating interactions between the fermions, and the quasimomentum is no longer an appropriate adiabatic parameter. Building on ideas of quantized charge pumping [94] and Hall conduction [95], one can obtain a many-body Berry phase by twisting the tunneling  $t \rightarrow te^{i\theta}$  that connects the boundaries and integrating over the twisting angle  $\theta$ . Interestingly, this concept can be

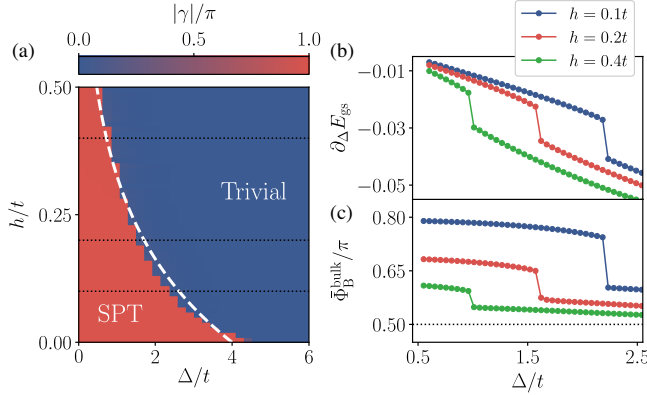


FIG. 4. Topological phase transitions. (a) Contour plot of the many-body Berry phase, which allows differentiating between the SPT with  $\gamma = \pi$  and the trivial band insulator (TBI) with  $\gamma = 0$ . The dashed line is obtained by fitting the critical points to an exponential (see main text). (b) First derivative of the ground-state energy  $\partial_{\Delta} E_{\text{gs}} = (E_{\text{gs}}(\Delta_1) - E_{\text{gs}}(\Delta_2))/(\Delta_1 - \Delta_2)$  with respect to the imbalance  $\Delta/t$  for different values of  $h/t$ . (c) Average Ising flux  $\Phi_{\text{B}}^{\text{bulk}}$  as a function of the imbalance  $\Delta/t$ . The calculations were performed directly in the thermodynamic limit for a half-filled ladder.

generalized to systems with hard-wall boundary conditions [96] since the twisting can actually be placed locally in any link that respects the underlying symmetry that protects the SPT phase, e.g., inversion symmetry in this case.

We have computed the many-body Berry phase (14) for an infinite Creutz-Ising ladder using the iDMRG algorithm [89], yielding the phase diagram of Fig. 4(a). The SPT phase is characterized by  $\gamma = \pi$  in the red region and is separated from a trivial band insulator (TBI) with  $\gamma = 0$  in the blue region by a critical line that reaches  $\Delta \approx 4t$  for  $h = 0$ . This case corroborates our previous interpretation (10) in terms of the mass-inversion point of the emergent Wilson fermions at  $\xi = \Delta/4t = 1$ . As the electric field  $h$  increases, this inversion point flows towards smaller values of the imbalance  $\Delta$ , which can be interpreted as a renormalization of the Wilson masses due to the interactions mediated by the gauge fields.

In this figure, we also show that the numerical critical line can be fitted to an exponential  $\xi_c = \xi_0 \exp\{-h/h_{\xi}\}$ , where  $h_{\xi}$  is a fitting parameter, and  $\xi_0 = 1$  is fixed by setting the critical point at  $\Delta/4t = 1$  for  $h = 0$ . Let us remark that this exponential behavior is consistent with the claim that the SPT phase and, in general, the Aharonov-Bohm instability and the flux-dominated phase persist to arbitrarily large values of the transverse  $h$  when the imbalance is  $\Delta = 0$ . For zero imbalance, the appearance of the flat bands described previously endows the SPT phase with an intrinsic robustness to the interactions mediated by the fluctuating gauge field.

Let us note that the critical line describes first-order topological phase transitions, as can be appreciated in

Fig. 4(b), where we display the derivative of the ground-state energy  $\partial_{\Delta} E_{\text{gs}}$  for three different values of electric-field strength [dotted lines of Fig. 4(a)]. The discontinuous jumps account for the first-order nature of the phase transitions. A similar discontinuity can be observed in the average magnetic flux (11), evaluated at the bulk of the ladder [Fig. 4(c)].

#### IV. TOPOLOGY FROM CONNECTIVITY

The topological properties described in the previous section are associated, loosely speaking, with the matter degrees of freedom since they are adiabatically connected to the static gauge field limit at  $h = 0$ —although matter and gauge are intertwined for any finite value of  $h$ . In this section, we focus on different topological effects that arise due to the dynamical nature of the gauge field. In particular, we provide quantitative evidence supporting the equivalence between the cross-linked ladder and a cylindrical geometry. This evidence allows us to interpret our model as the thin-cylinder limit of a 2D IGT and to identify various topological properties such as the ground-state degeneracy or the presence of topological order throughout the whole phase diagram. We also show that the intertwining of the matter and gauge fields in the SPT phase leads to a topological flux threading of the cylinder, and we give further arguments for its survival to arbitrary transverse fields.

##### A. Effective Creutz-Ising cylinder

Let us, momentarily, switch off the gauge-matter coupling and focus on the pure gauge theory  $\hat{H}_{\text{CI}}(0, 0, h, J)$  in Eq. (5). For  $h/J \rightarrow 0$  (with  $J > 0$ ), and for the sake of argument, we assume that  $|g\rangle$  is the single ground state in a flux-dominated phase with zero flux per plaquette  $\Phi_{\text{B}} = 0$ . We note that the following argument, first applied to the IGT on a square ladder [14], is also valid for  $\Phi_{\text{B}} = \pi$  in the case  $J < 0$ . As shown in Fig. 5(a), flipping the Ising fields via  $\sigma_{(ij)}^x$  creates a pair of  $\Phi_{\text{B}} = \pi$  excitations at neighboring plaquettes, which can be separated at the expense of flipping additional Ising fields along a path  $\Gamma_{\ell}$ . By extending this path towards the boundaries of the ladder, the  $\pi$  fluxes get expelled, and one recovers a state  $|\tilde{g}\rangle = \mathbf{D}_{\ell}|g\rangle$  with vanishing flux  $\Phi_{\text{B}} = 0$ , where

$$\mathbf{D}_{\ell} = \prod_{(ij) \in \Gamma_{\ell}} \sigma_{(ij)}^x \quad (15)$$

is the so-called Dirac string. Similarly to Eq. (3), one can define a four-point correlator involving Ising fields

$$\mathbf{B}_{\Gamma_{\dagger}} = \prod_{(ij) \in \Gamma_{\dagger}} \sigma_{(ij)}^z, \quad (16)$$

where  $\Gamma_{\dagger}$  is a vertical path that connects the two legs of the ladder. As demonstrated below,  $\Gamma_{\dagger}$  is equivalent to a path

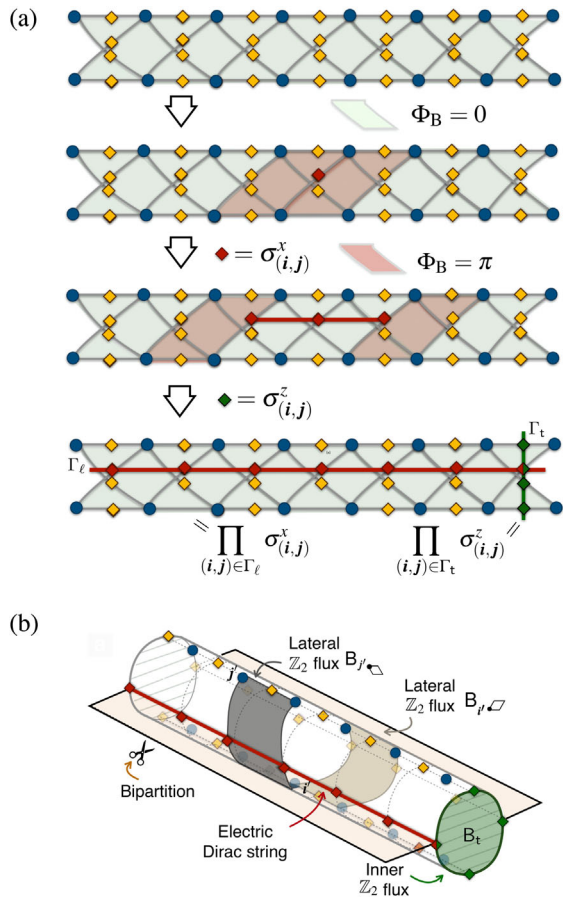


FIG. 5. Ground-state degeneracy of the Creutz-Ising cylinder. (a) In the  $h/J \rightarrow 0$  limit, the ground-state corresponds to the zero-flux state (green plaquettes), and excitations correspond to  $\pi$ -flux plaquettes (red) connected by an electric-field string (red line). By extending the string to the ladder edges, one recovers a different zero-flux ground state. (b) By considering the crossed-link tunnelings of the ladder as two different paths enclosing an area, the Creutz ladder can be represented as a thin-cylinder limit of a 2D LGT.

that wraps around a nontrivial cycle of a cylinder, such that the correlator (16) can be interpreted as a Wegner-Wilson loop operator measuring the flux threading the hole of the cylinder.

In the lowest panel of Fig. 5(a), one can see that the Dirac string shares only one common link with the four-point correlator and thus anticommutes,  $\{D_\ell, B_t\} = 0$ . Conversely, the Dirac string shares a pair of links with the trapezoidal plaquettes (3) and thus commutes with the Hamiltonian  $[\tilde{H}_{CI}(0, 0, h, J), D_\ell] = 0$ . As a consequence, if we assume that  $B_t|g\rangle = +|g\rangle$ , we immediately obtain  $B_t|\tilde{g}\rangle = -|\tilde{g}\rangle$ , whereas  $\tilde{H}_{CI}(0, 0, h, J)|\tilde{g}\rangle = E_{gs}|\tilde{g}\rangle$  and  $\tilde{H}_{CI}(0, 0, h, J)|g\rangle = E_{gs}|g\rangle$ . Accordingly, the two states are orthogonal and have the same energy  $E_{gs}$ . Our original assumption of a single ground state thus needs to be dropped in favor of the existence of a two-dimensional ground-state manifold spanned by  $\{|g\rangle, |\tilde{g}\rangle\}$ .

The presence of such a ground-state manifold can be a manifestation of topological order. As outlined in the Introduction, spin-liquid states with topological order can be characterized by a ground-state degeneracy that depends on the genus of the manifold in which they are defined [5]. The deconfined phase of the (2 + 1) IGT does indeed display this property, which is crucial in studies of fractionalization in high- $T_c$  superconductors [97,98]. In our case, the cross-linked tunnelings of Fig. 1 can be understood as a planar projection of the two paths that traverse the different faces of a thin cylinder [see Fig. 5(b)]. From this perspective, the four-point correlator (16) is actually a Wegner-Wilson loop that measures the inner  $\mathbb{Z}_2$  flux through the hole of the cylinder. As a consequence, the twofold degeneracy follows from the nontrivial topology of the manifold: The two states that span the ground-state manifold  $|g\rangle, |\tilde{g}\rangle$  have a vanishing flux  $\Phi_B = 0$  through the lateral surface of the cylinder, but only one of them,  $|\tilde{g}\rangle$ , has a  $\pi$  flux through the cylinder's hole. This ground-state  $|\tilde{g}\rangle$  is sometimes described as a state with a vison (i.e., vortex excitation) trapped within the hole of the cylinder.

In a finite-size system, at any small but nonzero  $h/J$ , the ground-state degeneracy is lifted, and the manifold splits into two eigenstates of  $D_\ell$  that amount to the symmetric and antisymmetric superpositions of  $|g\rangle$  and  $|\tilde{g}\rangle$ . In the thermodynamic limit, the gap in the ground-state manifold closes exponentially, and any small perturbation tends to select one of the two eigenstates of  $B_t$ , either  $|g\rangle$  or  $|\tilde{g}\rangle$ , which has a lower entanglement [99]. In particular, we note that MPS simulations with finite bond dimension favor  $|g\rangle, |\tilde{g}\rangle$  as ground states with respect to any other choice. Having less entanglement, their approximation for a fixed value of the bond dimension is more accurate, and thus their energy is lower than that of any other linear combination. Below, we show that this effect is also manifest in the presence of dynamical fermions and that the specific intertwining of gauge and matter fields in the SPT phase induces well-defined magnetic fluxes inside the cylinder.

## B. Magnetic fluxes and Ising susceptibility

We now explore the properties of the ground state as we depart from the limit  $h/J \rightarrow 0$ . For the pure-gauge case described above, in particular, a phase transition takes place at a finite value of  $h/J$ . As announced in Sec. II B, the cross-linked ladder geometry allows for a confinement-deconfinement phase transition akin to the (2 + 1) IGT [21]. This phase transition can be probed by the  $\mathbb{Z}_2$ -flux susceptibility  $\chi_B^{\text{bulk}} = \partial \bar{\Phi}_B^{\text{bulk}} / \partial h$ , evaluated through the magnetic flux (11) at the bulk of the ladder. It can be shown that, after a duality transformation, the pure-gauge Ising gauge theory is equivalent to the quantum Ising model in a transverse field [21]. In this picture, the  $\mathbb{Z}_2$ -flux susceptibility is equivalent to the susceptibility of the magnetization, which acts as an order parameter in the Ising model. We use iDMRG to obtain the approximation



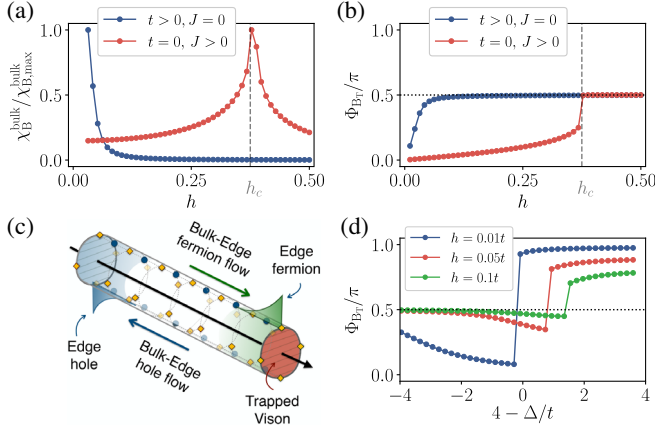


FIG. 6.  $\mathbb{Z}_2$  magnetic fluxes in the infinite Creutz-Ising cylinder. (a)  $\mathbb{Z}_2$ -flux susceptibility as a function of the electric-field strength. We compare the pure-gauge case, setting  $t = 0$  and  $J = 1$  (red circles), with the case in which the gauge fields interact with the fermionic matter, setting  $t = 1$ ,  $\Delta = 5t$ , and  $J = 0$  (blue circles). In the first case, the susceptibility shows a diverging peak, signaling a quantum phase transition between deconfined and confined phases. In the presence of dynamical matter, however, there is no apparent divergence hinting at the absence of such a transition. (b)  $\mathbb{Z}_2$  inner flux piercing the cylinder  $\Phi_{\mathbb{B}_t}$ . In the pure-gauge case (red circles), this inner flux displays nonanalytical behavior across a critical transverse field  $h_c$ . For dynamical matter (blue circles), this tendency is not abrupt, and the inner flux only attains the value  $\Phi_{\mathbb{B}_t} \approx \pi/2$  asymptotically without any nonanalyticity. (c) Topological flux threading relating the existence of edge states to a trapped vison inside the cylinder. (d) Similarly to the Berry phase  $\gamma$ , the inner flux  $\Phi_{\mathbb{B}_t}$  changes from 0 to  $\pi$  as one crosses the critical point separating TBI and SPT. The deviations from those precise values are due to quantum fluctuations.

of the ground state of the system defined on an infinitely long ladder as a MPS. The system is thus equivalent to a  $2 \times \infty$  cylinder: the thin-cylinder limit of a  $2 + 1$  fermionic IGT. The maximum bond dimension we have used is  $D = 200$ , testing that it is sufficient to achieve a good convergence. As clearly evidenced by the iDMRG results of Fig. 6(a) (red circles), there is a peak in the  $\mathbb{Z}_2$  susceptibility, whose height actually diverges with the ladder size at the critical coupling  $h/J|_c$ . In Fig. 6(b), we plot the value of the inner flux  $\Phi_{\mathbb{B}_t} = \arccos(\langle \mathbb{B}_t \rangle)$  through the hole of the effective cylinder as a function of the transverse field  $h$  (red circles). The plot shows that, in the  $h/J \rightarrow 0$  limit, the cylinder has zero inner flux  $\Phi_{\mathbb{B}_t} = 0$ , and the ground state is  $|g\rangle$  as anticipated. By increasing the transverse field, quantum fluctuations change the inner flux, which acts as a nonlocal order parameter for the transition to the confined phase displaying a nonanalytical behavior as we cross  $h/J|_c$ .

Let us now switch on the gauge-matter coupling and see how this picture gets modified by the inclusion of dynamical fermions governed by  $\tilde{H}_{\text{CI}}(t, \Delta, h, 0)$  in Eq. (5). First of

all, we find that there is no peak in the  $\mathbb{Z}_2$  susceptibility for any value of  $h$  [see blue circles of Fig. 6(a)], which suggests the absence of a phase transition. Furthermore, we plot the value of the inner flux in Fig. 6(b), which again attains the value  $\Phi_{\mathbb{B}_t} = 0$  in the  $h/t \rightarrow 0$  limit (blue circles). The zero inner-flux state can be understood as the generalization of the  $|g\rangle$  ground state to a situation that encompasses dynamical fermions intertwining with the Ising fields. As neatly depicted, the  $\mathbb{Z}_2$  flux changes smoothly from  $\Phi_{\mathbb{B}_t} = 0 \rightarrow \pi/2$  as the electric-field strength is increased. Therefore, the absence of nonanalyticities again suggests that there is a single flux-dominated phase for arbitrary transverse fields. Although here we did not show that, for a cylindrical geometry and in the presence of fermionic matter, this phase exhibits a degenerate ground-state manifold, we will argue at the end of the section that this is indeed the case using the topological entanglement entropy. Moreover, in the last section, we will demonstrate that, in this phase, fermionic matter is deconfined.

### C. Trapped visons from topological flux threading

As discussed above for the pure-gauge limit, topological order becomes manifest through the twofold ground-state degeneracy  $\{|g\rangle, |\tilde{g}\rangle\}$  and the absence or presence of a trapped vison. Yet, in the previous section [see Fig. 6(b)], we have only found the dynamical-fermion generalization of  $|g\rangle$ . As described in Sec. III, the Aharonov-Bohm instability can lead to a SPT ground-state or to a trivial band insulator [see Fig. 4(a)]. We now discuss the difference between the intertwining of the gauge and matter fields in these two cases, and we unveil a very interesting interplay between the topological degeneracy and the existence of edge states in the SPT phase.

To understand this interplay, let us recall Laughlin's argument for the quantum Hall effect [100], which states that a single charge is transferred between the edges of a quantum Hall cylinder when a magnetic flux quantum is threaded through its hole. In the Creutz-Ising ladder, one can move from the TBI onto the SPT ground state by gradually decreasing the imbalance  $\Delta$ . As the system crosses the critical point, topological edge states will appear at the boundaries of the ladder, which can be seen as the result of charge being transferred from the bulk to the edges [see Fig. 6(c)]. In contrast to Laughlin's pumping, where it is the external variation of the flux that leads to charge transport, here it is the transition into a topological phase and the associated charge transfer that should generate a nonvanishing  $\mathbb{Z}_2$  inner flux. In Fig. 6(d), we confirm this behavior and show that the  $\mathbb{Z}_2$  inner flux changes from  $\Phi_{\mathbb{B}_t} \approx 0$  (TBI) to  $\Phi_{\mathbb{B}_t} \approx \pi$  (SPT) at fixed  $h = 0.01t$ .

This effect can be understood as a topological flux threading, where the existence of edge states gets intertwined with the trapping of a vison through the cylinder's hole, giving access to the dynamical-fermion generalization of  $|\tilde{g}\rangle$ . We note that this phenomenon cannot be observed

with a background static field, such as the magnetic field of the quantum Hall effect, but is instead characteristic of LGTs with fermionic matter, unveiling an interesting interplay between the Berry phase and the inner  $\mathbb{Z}_2$  flux. This case offers a neat alternative to the numerical demonstration of the twofold ground-state degeneracy, typically hindered by finite-size effects. As the quantum fluctuations are increased by raising  $h$ , we see that one tends smoothly to the electric-field-dominated phase  $\Phi_{B_1} = \pi/2$ , but the first-order topological phase transition between SPT and TBI, and the intertwining of the edge and vison states are still captured by the discontinuity of the inner flux.

#### D. Topological entanglement entropy

As argued in the previous section, the ground-state degeneracy and the flux threading are topological phenomena related to the underlying cylindrical manifold, which raises the possibility that this quasi-1D IGT (5) displays topological order, as occurs for Kitaev's toric code [8]. This is indeed the case in other quasi-1D geometries, such as the thin-torus limit of two-dimensional fractional quantum Hall states [101–103]. In recent years, quantum-information tools that quantify the entanglement of the ground state have turned out to be extremely useful to characterize various many-body properties [104]. In particular, the von Neumann entanglement entropy for a bipartition of the ground-state  $|g\rangle$  into two blocks  $A - B$  of equal size is defined as  $S(\rho_A) = -\text{Tr}\{\rho_A \log \rho_A\}$ , where  $\rho_A = \text{Tr}_B\{|g\rangle\langle g|\}$  is the reduced density matrix. For a  $(2 + 1)$  topologically ordered ground state, this entanglement entropy scales as

$$S(\rho_t) = \alpha|\partial A| - \gamma_t, \quad (17)$$

where  $|\partial A|$  is the number of sites that belong to the boundary separating the  $A$ - $B$  regions,  $\alpha$  is a constant that characterizes this entanglement area law, while  $\gamma_t$  is a universal subleading constant that quantifies the topological corrections [72,73]. Although in a gapped phase the value of  $\gamma_t$  is constant, it has already been observed that, close to a QPT, there are strong finite-size effects, and from numerical simulation, it is very hard to extract a reliable determination of it [105]. Furthermore, the value of  $\gamma_t$  for bipartitions that are not contractible to a point depends on both the choice of the bipartition and the choice of the ground state in the ground-state manifold [99].

In order to reliably extract  $\gamma_t$ , we turn to study finite-size Creutz-Ising ladders, interpreted through the mapping to the thin cylinder of length  $2 \times N_s$  of Fig. 5(b). We consider a bipartition separating the two legs, such that  $|\partial A| = N_s$ . In the effective manifold, this corresponds to a longitudinal bipartition of the cylinder [see Fig. 5(b)], such that the entropy (17) should scale with the length of the cylinder. In this finite-size regime, the ground state is an eigenstate of  $D_\ell$  and thus has minimal entropy. Thus,  $\gamma_t$  should get

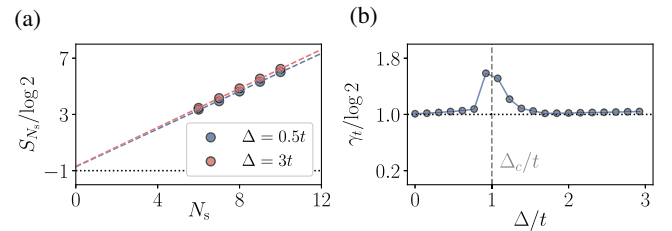


FIG. 7. Topological entanglement in the Creutz-Ising ladder. (a) Scaling of the entanglement entropy  $S_{N_s}$  with  $N_s$  setting  $h = 0.02t$ , and for different imbalances corresponding to the SPT ( $\Delta = 0.5t$ ) and TBI ( $\Delta = 3t$ ) phases. In both cases, the topological correction to the entanglement entropy is  $\gamma_t = \log 2$ , signaling topological order. In panel (b), we represent this quantity as a function of  $\Delta/t$ . The grey dashed line denotes the position of the first-order transition for a finite cylinder of length  $N_s = 10$ .

saturated at its maximum value, namely,  $\gamma_t = \log(2)$ . Our numerical analysis is limited to short ladders, as the particular bipartition limits the efficiency of the MPS routines. In Fig. 7(a), we plot the entanglement entropy as a function of the ladder length for two points deep in the SPT and the TBI. The fit of the data allows us to confirm that  $\gamma_t \approx \log 2$  in both the SPT and TBI phases. After repeating the same analysis for several values of the imbalance, we obtain Fig. 7(b). In this figure,  $\gamma_t$  is constantly very close to the expected  $\log(2)$  within both the SPT and TBI phases. It only departs significantly from that value close to the phase transition, where the larger correlation length increases the finite-size effects [105]. The presence of a nonzero topological entropy is a further indication that the complete gauge-matter system is topologically ordered both in the SPT phase and in the TBI. Because of the lack of signature of criticality in our numerical results about the fluxes threading the cylinder and the bulk susceptibility of Figs. 6(a) and 6(b) (blue circles), we are thus confident that the topologically ordered phase survives for large values of the electric field.

## V. $\mathbb{Z}_2$ FERMIONIC DECONFINEMENT

In this section, we argue that the topologically ordered flux-dominated phase described above shows fermionic deconfinement for any value of the transverse field. We first introduce the notion of gauge frustration and how it generates deconfined topological defects when the system is doped above or below half-filling. We then quantitatively characterize the absence of confinement using static charges, and we compare it with the more standard case involving string breaking.

### A. Gauge frustration and topological defects

Paralleling the situation in the standard  $(2 + 1)$  IGT [14], the existence of topological order in the Creutz-Ising

ladder suggests that the ground state lies in a deconfined phase despite the lack of plaquette interactions  $J = 0$ . As outlined above, the absence of criticality for large  $h$  suggests that this deconfinement may survive to arbitrarily large electric-field strengths, which is in contrast to the standard IGT [12].

Let us start by discussing the half-filled regime of the Hamiltonian (5) for  $h \gg t$  and  $\Delta = 0$ . In this case, the link Ising fields minimize their energy for  $|+\rangle = (|\uparrow\rangle + |\downarrow\rangle)/\sqrt{2}$ . However, the presence of fermions can frustrate some links in order to satisfy the constraints (6), forcing the Ising fields to lie in  $|-\rangle = (|\uparrow\rangle - |\downarrow\rangle)/\sqrt{2}$ . We call this gauge frustration, namely, the impossibility of simultaneously minimizing all the individual Hamiltonian terms due to the Gauss constraint.

In contrast to pure gauge theories, this type of frustration can occur in the even sector  $q_i = 0$ , as some of the sites might be occupied by a dynamical fermion [see Fig. 8(a)]. By plotting only the frustrated links or bonds, one understands that the ground state corresponds to a partial covering of the ladder with a single restriction: Each site can be touched by one bond at most [see Fig. 8(b)]. This is precisely the definition of a dimer, with the peculiarity that dimer models typically consider the complete covering of the lattice [106,107], whereas in our half-filled case, the ground state will be a linear superposition of all partial dimer coverings. We note that, in the absence of dynamical fermions, the original connection of an IGT to a quantum dimer model in the large- $h$  limit was put forth by Moessner *et al.* by introducing a static background  $\mathbb{Z}_2$  charge  $q_i = 1$  at every site (i.e., odd-charge sector) [108]. In our case, the dynamical fermions allow for this dimer limit even in the absence of static charges, albeit only with partial coverings.

So far, the imbalance has been fixed to zero. If we now allow for  $\Delta > 0$ , the fermions will preferably occupy the lower leg, such that only two degenerate coverings are relevant for the large- $h$  ground state [see Fig. 8(c)]. These two coverings, which we label as A and B, are related by a simple lattice translation and, yet, they are essential for the deconfinement of the Creutz-Ising ladder. If one adds a pair of fermions at a distance  $L$  above half-filling, these coverings must be accommodated in the upper leg, such that the Ising fields change to comply with the Gauss constraints. As depicted in Fig. 8(d), if we insist on maintaining one of the dimer coverings, say A, an electric-field string must connect the fermions in the upper leg, such that the energy is  $E(L) - E_0 = hL$ , and the charges are confined,  $V(L) \propto L$ . This case is the standard situation in the  $(2+1)$  IGT in the even sector [12]. In our case, however, the twofold coverings allow for a different situation: One can interpolate between the A and B configurations, such that  $E(L) - E_0 = 3h$ , and the charges are deconfined,  $V(L) \propto V_0$ . The charges, which are no longer confined in pairs but localized at the topological soliton that

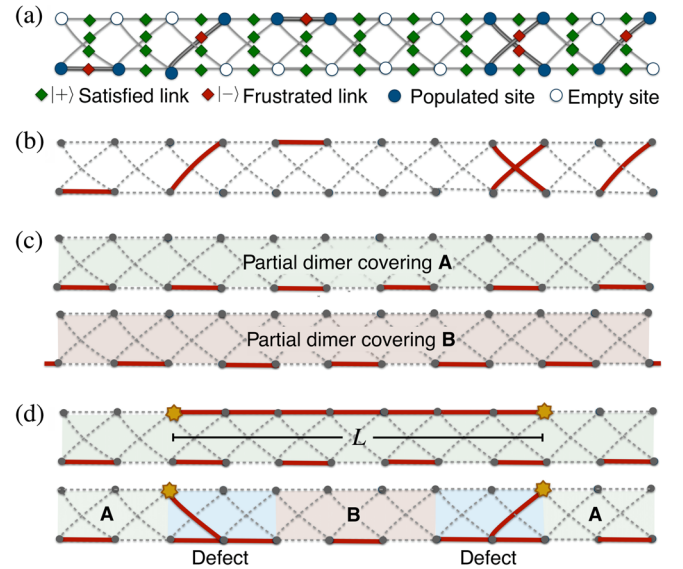


FIG. 8. Dimer coverings and soliton deconfinement. (a) In the  $h \gg t$ ,  $J$  and  $\Delta = 0$  limit, Gauss law requires that some of the Ising fields are frustrated due to the distribution of fermionic matter in the ladder. (b) The frustrated Ising fields can be identified with dimers (red bonds) that partially cover the lattice. (c) Switching on  $\Delta > 0$  selects only the A and B dimer coverings. (d) Adding two fermions changes the dimer covering, and it becomes energetically favorable to create topological defects in the dimer configurations, which can accommodate for the deconfined charges.

interpolates between A and B, carry a nonzero  $\mathbb{Z}_2$  charge, which is at the very heart of the notion of deconfinement.

To assess the validity of these arguments and extend them beyond the  $h \gg t$  limit, we explore the Creutz-Ising ladder for finite doping using the MPS numerics. In Fig. 9(a), we depict the occupation  $\bar{n}_{i_1} = \langle :n_{(i_1,0)}: \rangle + \langle :n_{(i_1,1)}: \rangle$  summed over the pair of sites in the upper and lower legs. This density displays an inversion-symmetric distribution of the extra doped charges, which are localized around distant centers, maximizing their corresponding distances. In Fig. 9(b), we represent the integrated  $\mathbb{Z}_2$  charge from the left boundary of the ladder  $Q_{i_1} = \sum_{j_1 \leq i_1} \bar{n}_{j_1}$ . Comparing this profile to Fig. 9(c), where we represent the electric-field configuration, it becomes manifest that each of the doped fermions is localized within a topological soliton of the gauge fields. The bound fermion-soliton quasiparticles are deconfined, as they carry a unit  $\mathbb{Z}_2$  charge [Fig. 9(b)] and can interact among each other forming a crystalline structure [Fig. 9(a)]. To the best of our knowledge, our results quantitatively confirm this mechanism for the first time and show that it can also appear in fermionic LGTs that combine topological order and SPT phases. We note that a similar deconfinement mechanism has been suggested for the odd sector of a pure IGT in  $(1+1)$  dimensions [108], based on an analogy to

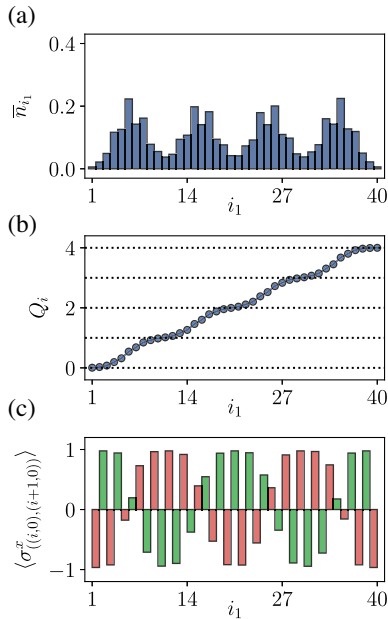


FIG. 9. Finite doping and soliton-induced deconfinement. (a) Real-space fermionic occupation for a ladder of length  $N_s = 40$  filled with  $N = 44$  particles for  $\Delta = 4t$ ,  $h = 0.2t$ , and  $J = 0$ , where the formation of a periodic crystalline structure can be appreciated. (b) Integrated charge  $Q_i$  along the ladder, showing that each peak of excess charge with respect to half-filling contains a fermionic number of one. (c) Corresponding electric-field configuration  $\langle \sigma_{((i,0),(i+1,0))}^x \rangle$  in the lower leg of the ladder; odd links are red, and even ones are green. Topological solitons between the two degenerate electric-field configurations appear, and the peaks of excess charge are located at the position of the defects.

the Peierls solitons in polymers [85]. Our detailed analysis shows that, in our case, these types of solitons, characterized by charge fractionalization [91,109,110], are not the underlying mechanism explaining the deconfinement for the  $h \gg t$  limit of IGTs. As discussed above, the integrated charge around the solitons is quantized in units of the  $\mathbb{Z}_2$  charge, but there is no signature of charge fractionalization [Fig. 9(b)]. This result points to a different nature of topological defects in the magnetic- and electric-dominated phases, which will be the subject of detailed future studies.

## B. Deconfinement versus string breaking

In this last section, we argue that the appearance of the mechanism of soliton deconfinement depends on the particular charge sector (6). So far, we have focused on the even sector, which is characterized by the absence of background  $\mathbb{Z}_2$  charges  $q_i = 0$ ,  $\forall i \in \mathbb{Z}_{N_s} \times \mathbb{Z}_2$ . We now make a full comparison with a different sector, hereby referred to as the imbalanced sector, where there is a static  $\mathbb{Z}_2$  charge at each site of the lower leg, namely,  $q_{(i,0)} = 1$ ,  $q_{(i,1)} = 0 \forall i \in \mathbb{Z}_{N_s}$ . In this case, there are neither frustrated bonds in the ground state nor partial dimer coverings or solitons as in Fig. 8. Accordingly, the situation and the confinement properties change completely. To quantify these differences, we introduce two additional background charges on the upper leg of the ladder that are separated by a distance  $L$ ; namely, we add  $q_{(i_0,1)} = q_{(i_0+L,1)} = 1$  to the two different charge sectors.

In Figs. 10(a)–10(b), we represent the total integrated charge  $\tilde{Q}_{i_1} = Q_{i_1} + \sum_{j_1 < i_1} (q_{(j_1,0)} + q_{(j_1,1)})$ , which includes both the dynamical fermions and the back-

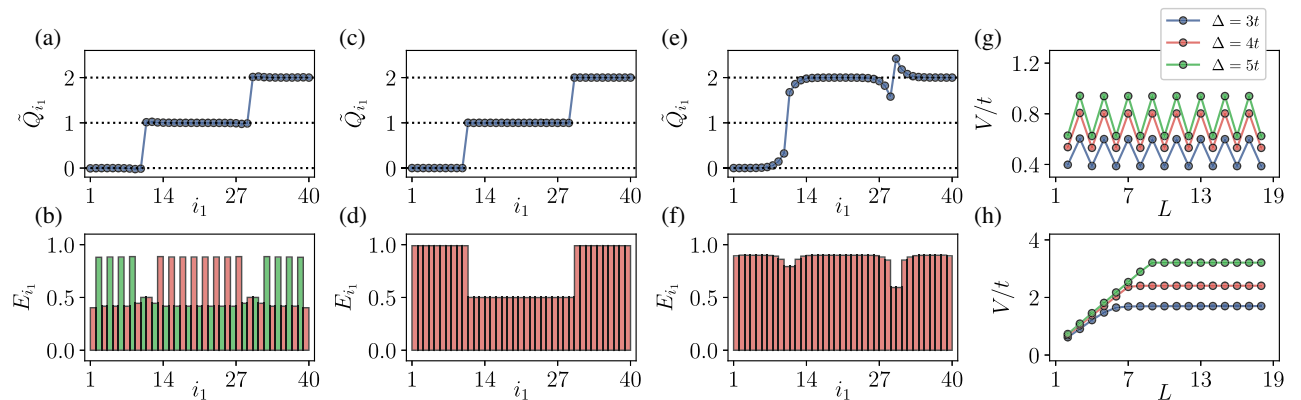


FIG. 10. Deconfinement versus string breaking. Panels (a)–(f) represent the ground-state configuration corresponding to a ladder of length  $N_s = 40$  at half-filling with two extra static charges located in the upper leg and separated by  $L = 20$  sites, with  $h = 0.2t$ . (a) Integrated total charge  $Q_i$  in the even-charge sector for  $\Delta = 3t$ , showing two jumps of height one at the location of the static charges. (b) Each static charge creates a defect electric field to satisfy Gauss law. (c) Same as before but for the imbalanced sector with  $\Delta = 10t$ . (d) In this case, an electric string develops between the charges. Panels (e) and (f) depict how, for  $\Delta = 3t$  and in the imbalanced sector, a particle-antiparticle pair is created in the vacuum to screen the static charges, breaking the original string between them. (g) Potential energy  $V/t$  between the two static charges as a function of the distance  $x$  between them, for different values of  $\Delta$ , in the even-charge sector. (h) A similar calculation in the imbalanced sector.

ground charges above the even-charge sector. We also depict the underlying averaged electric field,  $E_{i_1} = \sum_{i_2, i_2'} \langle \sigma_{((i_1, i_2), (i_1+1, i_2'))}^x \rangle / 4$ . The situation is analogous to the soliton-induced deconfinement discussed in the previous section, but the location of each soliton is now pinned to the position of the extra static charge, while in Fig. 9, the unpinned solitons tend to maximize their spread and distance, forming a soliton lattice. In Figs. 10(c)–10(d), we depict the same observables for the imbalanced sector. It is clear that an electric-field line connecting the static charges is established, which leads to the aforementioned confinement. The new aspect brought by the dynamical matter is that, by lowering the energy imbalance  $\Delta$ , it can become energetically favorable to create a particle-antiparticle pair that breaks this string and screens the static  $\mathbb{Z}_2$  charges, as can be observed in Figs. 10(e) and 10(f). In these figures, one sees that the electric fields are restricted to the regions around the static charges and that the  $\mathbb{Z}_2$  charges are no longer unity but get screened to  $\tilde{Q}_i \bmod 2 = 0$ , signaling the aforementioned string breaking.

We can make a quantitative study of the difference in the confinement properties of the two charge sectors by calculating the dependence of the effective potential with the distance between the static charges  $V(L)$ . In Fig. 10(g), we present the results for the even-charge sector and different values of  $\Delta$ . In all cases, apart from an even-odd effect due to the so-called Peierls-Nabarro barriers associated with the defects [111,112], the energy does not grow with the distance, signaling deconfinement. In contrast, in the imbalanced sector of Fig. 10(h), the potential grows linearly with the distance until the string breaks at a certain length, signaling confinement.

## VI. CONCLUSIONS AND OUTLOOK

In this work, we have identified novel topological effects in finite-density fermionic gauge theories. In particular, we introduce a minimal fermionic  $\mathbb{Z}_2$  lattice gauge theory, the Creutz-Ising ladder, which allows us to investigate the interplay between topology and gauge invariance. We show how, even in the absence of a plaquette term, the system presents a magnetic-flux-dominated phase, in which a dynamical  $\pi$  flux appears in the ground state as a consequence of an Aharonov-Bohm instability. This phenomenon results from the interplay between gauge-invariant interactions and the particular connectivity of the model, which also gives rise to SPT phases in the fermionic sector. We characterize the properties of these phases, including the presence of protected gauge-matter edge states, through MPS-based numerical calculations, and use a topological invariant to find first-order phase transitions between the topological and trivial phases.

Our model can also be interpreted as a thin-cylinder limit of a  $(2+1)$   $\mathbb{Z}_2$  LGT. This equivalence allows us to uncover the presence of topological order by calculating the topological correction to the entanglement entropy. Topological order is also associated with the degeneracy of the ground state, which can be characterized by two different fluxes threading the hole of the cylinder (i.e., presence or absence of a trapped vison). We have shown that, in the Creutz-Ising ladder, the topological order intertwines with topological symmetry protection, and this connection manifests in the change of the inner flux, and thus the trapping of a vison, when crossing phase transition lines towards the SPT phase such that edge states emerge from the bulk and localize within the ladder boundaries. This feature could facilitate the detection of topological order in future experiments.

Finally, we show how fermionic deconfinement, which accompanies the topologically order phase, survives for the whole parameter space considered. The deconfinement survives because of the presence of deconfined topological defects associated with the fermionic quasiparticles, which appear on a frustrated background of electric fields imposed by gauge invariance. We investigate this mechanism using both static and dynamical charges and compare it to the more standard confining case where string breaking usually takes place.

We believe that our results substantially advance the understanding of topological phenomena in lattice gauge theories. Moreover, we have shown that the inclusion of dynamical fermions can stabilize a magnetic-dominated deconfined phase even in the absence of plaquette interactions. Therefore, our work identifies a new avenue for the realization of spin-liquid physics in LGTs, relevant for both condensed matter and high-energy physics, in cold-atom experiments based on state-of-the-art building blocks that have already been used for quantum simulation purposes. This avenue would allow us to investigate complex phenomena, such as topological order and deconfinement, using minimal resources. The methods applied here can be used to further explore the static and dynamical properties of  $\mathbb{Z}_2$  fermionic gauge theories, including the phase diagram at different fillings or the nonequilibrium quench dynamics.

## ACKNOWLEDGMENTS

We acknowledge interesting discussions with L. Barbiero, M. Di Liberto, N. Goldman, S. Hands, V. Kasper, and E. Tirrito. This project has received funding from the European Union's Horizon 2020 research and innovation programme under the Marie Skłodowska-Curie Grant Agreement No. 665884, the Spanish Ministry MINECO and State Research Agency AEI (FISCATEAMO, FIDEUA PID2019-106901GB-I00/10.13039/501100011033, SEVERO OCHOA No. SEV-2015-0522 and No. CEX2019-000910-S, FPI), European

Social Fund, Fundaci Cellex, Generalitat de Catalunya (AGAUR Grant No. 2017 SGR 1341, CERCA/Program), ERC AdG NOQIA, EU FEDER, and the National Science Centre, Poland-Symfonia Grant No. 2016/20/W/ST4/00314. A. B. acknowledges support from the Ramón y Cajal program RYC-2016-20066, CAM/FEDER Project S2018/TCS- 4342 (QUITEMADCM), and PGC2018-099169-B-I00 (MCIU/AEI/FEDER, UE). L. T. acknowledges support from the Ramón y Cajal program RYC-2016-20594 and the “Plan Nacional Generación de Conocimiento” PGC2018-095862-B-C22.

- 
- [1] L. Landau, *On the Theory of Phase Transformations*, Zh. Eksp. Teor. Fiz. **7**, 19 (1937) [Ukr. J. Phys. **1**, 234 (1969)], <https://web.archive.org/web/20151214124950/http://www.ujp.bitp.kiev.ua/files/journals/53/si/53SI08p.pdf>.
- [2] P. W. Anderson, *The Resonating Valence Bond State in  $\text{La}_2\text{CuO}_4$  and Superconductivity*, *Science* **235**, 1196 (1987).
- [3] G. Misguich, *Quantum Spin Liquids, Exact Methods in Low-Dimensional Statistical Physics and Quantum Computing: Lecture Notes of the Les Houches Summer School* (2010), Vol. 89, p. 431, <https://global.oup.com/academic/product/exact-methods-in-low-dimensional-statistical-physics-and-quantum-computing-9780199574612?cc=us&lang=en&>.
- [4] L. Balents, *Spin Liquids in Frustrated Magnets*, *Nature (London)* **464**, 199 (2010).
- [5] X.-G. Wen, *Colloquium: Zoo of Quantum-Topological Phases of Matter*, *Rev. Mod. Phys.* **89**, 041004 (2017).
- [6] A. Kitaev and J. Preskill, *Topological Entanglement Entropy*, *Phys. Rev. Lett.* **96**, 110404 (2006).
- [7] M. Levin and X.-G. Wen, *Detecting Topological Order in a Ground State Wave Function*, *Phys. Rev. Lett.* **96**, 110405 (2006).
- [8] A. Yu. Kitaev, *Fault-Tolerant Quantum Computation by Anyons*, *Ann. Phys. (Amsterdam)* **303**, 2 (2003).
- [9] C. Nayak, S. H. Simon, A. Stern, M. Freedman, and S. D. Sarma, *Non-Abelian Anyons and Topological Quantum Computation*, *Rev. Mod. Phys.* **80**, 1083 (2008).
- [10] T.-H. Han, J. S. Helton, S. Chu, D. G. Nocera, J. A. Rodriguez-Rivera, C. Broholm, and Y. S. Lee, *Fractionalized Excitations in the Spin-Liquid State of a Kagome-Lattice Antiferromagnet*, *Nature (London)* **492**, 406 (2012).
- [11] J. Wen, S.-L. Yu, S. Li, W. Yu, and J.-X. Li, *Experimental Identification of Quantum Spin Liquids*, *npj Quantum Mater.* **4**, 12 (2019).
- [12] J. B. Kogut, *An Introduction to Lattice Gauge Theory and Spin Systems*, *Rev. Mod. Phys.* **51**, 659 (1979).
- [13] S. Elitzur, *Impossibility of Spontaneously Breaking Local Symmetries*, *Phys. Rev. D* **12**, 3978 (1975).
- [14] E. Fradkin, *Field Theories of Condensed Matter Physics*, 2nd ed. (Cambridge University Press, Cambridge, England, 2013).
- [15] G. Baskaran and P. W. Anderson, *Gauge Theory of High-Temperature Superconductors and Strongly Correlated Fermi Systems*, *Phys. Rev. B* **37**, 580 (1988).
- [16] N. Read and S. Sachdev, *Large- $N$  Expansion for Frustrated Quantum Antiferromagnets*, *Phys. Rev. Lett.* **66**, 1773 (1991).
- [17] J. Kogut and L. Susskind, *Hamiltonian Formulation of Wilson’s Lattice Gauge Theories*, *Phys. Rev. D* **11**, 395 (1975).
- [18] C. N. Yang and R. L. Mills, *Conservation of Isotopic Spin and Isotopic Gauge Invariance*, *Phys. Rev.* **96**, 191 (1954).
- [19] J. Greensite, *An Introduction to the Confinement Problem* (Springer, New York, 2011).
- [20] K. G. Wilson, *Confinement of Quarks*, *Phys. Rev. D* **10**, 2445 (1974).
- [21] F. J. Wegner, *Duality in Generalized Ising Models and Phase Transitions without Local Order Parameters*, *J. Math. Phys. (N.Y.)* **12**, 2259 (1971).
- [22] B. M. Terhal, *Quantum Error Correction for Quantum Memories*, *Rev. Mod. Phys.* **87**, 307 (2015).
- [23] S. Trebst, P. Werner, M. Troyer, K. Shtengel, and C. Nayak, *Breakdown of a Topological Phase: Quantum Phase Transition in a Loop Gas Model with Tension*, *Phys. Rev. Lett.* **98**, 070602 (2007).
- [24] A. Hamma and D. A. Lidar, *Adiabatic Preparation of Topological Order*, *Phys. Rev. Lett.* **100**, 030502 (2008).
- [25] J. Vidal, S. Dusuel, and K. P. Schmidt, *Low-Energy Effective Theory of the Toric Code Model in a Parallel Field*, *Phys. Rev. B* **79**, 033109 (2009).
- [26] L. Tagliacozzo and G. Vidal, *Entanglement Renormalization and Gauge Symmetry*, *Phys. Rev. B* **83**, 115127 (2011).
- [27] E. Fradkin and S. H. Shenker, *Phase Diagrams of Lattice Gauge Theories with Higgs Fields*, *Phys. Rev. D* **19**, 3682 (1979).
- [28] J. Vidal, R. Thomale, K. P. Schmidt, and S. Dusuel, *Self-Duality and Bound States of the Toric Code Model in a Transverse Field*, *Phys. Rev. B* **80**, 081104 (2009).
- [29] I. S. Tupitsyn, A. Kitaev, N. V. Prokof’ev, and P. C. E. Stamp, *Topological Multicritical Point in the Phase Diagram of the Toric Code Model and Three-Dimensional Lattice Gauge Higgs Model*, *Phys. Rev. B* **82**, 085114 (2010).
- [30] F. F. Assaad and T. Grover, *Simple Fermionic Model of Deconfined Phases and Phase Transitions*, *Phys. Rev. X* **6**, 041049 (2016).
- [31] S. Gazit, M. Randeria, and A. Vishwanath, *Emergent Dirac Fermions and Broken Symmetries in Confined and Deconfined Phases of  $\mathbb{Z}_2$  Gauge Theories*, *Nat. Phys.* **13**, 484 (2017).
- [32] C. Prosko, S.-P. Lee, and J. Maciejko, *Simple  $\mathbb{Z}_2$  Lattice Gauge Theories at Finite Fermion Density*, *Phys. Rev. B* **96**, 205104 (2017).
- [33] S. Gazit, F. F. Assaad, S. Sachdev, A. Vishwanath, and C. Wang, *Confinement Transition of 2 Gauge Theories Coupled to Massless Fermions: Emergent Quantum Chromodynamics and  $SO(5)$  Symmetry*, *Proc. Natl. Acad. Sci. U.S.A.* **115**, E6987 (2018).

- [34] E. J. Knig, P. Coleman, and A. M. Tsvelik, *Soluble Limit and Criticality of Fermions in  $\mathbb{Z}_2$  Gauge Theories*, arXiv:1912.11106.
- [35] M. Lewenstein and A. Sanpera, *Ultracold Atoms in Optical Lattices Simulating Quantum Many-Body Systems* (Oxford University Press, Oxford, England, 2012).
- [36] I. Bloch, J. Dalibard, and W. Zwerger, *Many-Body Physics with Ultracold Gases*, *Rev. Mod. Phys.* **80**, 885 (2008).
- [37] M. C. Banuls, R. Blatt, J. Catani, A. Celi, J. I. Cirac, M. Dalmonte, L. Fallani, K. Jansen, M. Lewenstein, S. Montangero, C. A. Muschik, B. Reznik, E. Rico, L. Tagliacozzo, K. Van Acoleyen, F. Verstraete, U. J. Wiese, M. Wingate, J. Zakrzewski, and P. Zoller, *Simulating Lattice Gauge Theories within Quantum Technologies*, arXiv:1911.00003.
- [38] U.-J. Wiese, *Ultracold Quantum Gases and Lattice Systems: Quantum Simulation of Lattice Gauge Theories*, *Ann. Phys. (Berlin)* **525**, 777 (2013).
- [39] E. Zohar, J. I. Cirac, and B. Reznik, *Quantum Simulations of Lattice Gauge Theories Using Ultracold Atoms in Optical Lattices*, *Rep. Prog. Phys.* **79**, 014401 (2015).
- [40] M. Dalmonte and S. Montangero, *Lattice Gauge Theory Simulations in the Quantum Information Era*, *Contemp. Phys.* **57**, 388 (2016).
- [41] H. P. Büchler, M. Hermele, S. D. Huber, M. P. A. Fisher, and P. Zoller, *Atomic Quantum Simulator for Lattice Gauge Theories and Ring Exchange Models*, *Phys. Rev. Lett.* **95**, 040402 (2005).
- [42] T. Byrnes and Y. Yamamoto, *Simulating Lattice Gauge Theories on a Quantum Computer*, *Phys. Rev. A* **73**, 022328 (2006).
- [43] E. Zohar and B. Reznik, *Confinement and Lattice Quantum-Electrodynamics Electric Flux Tubes Simulated with Ultracold Atoms*, *Phys. Rev. Lett.* **107**, 275301 (2011).
- [44] E. Zohar, J. I. Cirac, and B. Reznik, *Simulating Compact Quantum Electrodynamics with Ultracold Atoms: Probing Confinement and Nonperturbative Effects*, *Phys. Rev. Lett.* **109**, 125302 (2012).
- [45] E. Zohar, J. I. Cirac, and B. Reznik, *Cold-Atom Quantum Simulator for  $SU(2)$  Yang-Mills Lattice Gauge Theory*, *Phys. Rev. Lett.* **110**, 125304 (2013).
- [46] D. Banerjee, M. Bögli, M. Dalmonte, E. Rico, P. Stebler, U.-J. Wiese, and P. Zoller, *Atomic Quantum Simulation of  $U(n)$  and  $SU(n)$  Non-Abelian Lattice Gauge Theories*, *Phys. Rev. Lett.* **110**, 125303 (2013).
- [47] L. Tagliacozzo, A. Celi, P. Orland, M. W. Mitchell, and M. Lewenstein, *Simulation of Non-Abelian Gauge Theories with Optical Lattices*, *Nat. Commun.* **4**, 2615 (2013).
- [48] L. Tagliacozzo, A. Celi, A. Zamora, and M. Lewenstein, *Optical Abelian Lattice Gauge Theories*, *Ann. Phys. (N.Y.)* **330**, 160 (2013).
- [49] E. Zohar, A. Farace, B. Reznik, and J. I. Cirac, *Digital Quantum Simulation of  $\mathbb{Z}_2$  Lattice Gauge Theories with Dynamical Fermionic Matter*, *Phys. Rev. Lett.* **118**, 070501 (2017).
- [50] A. Bermudez and D. Porras, *Interaction-Dependent Photon-Assisted Tunneling in Optical Lattices: A Quantum Simulator of Strongly-Correlated Electrons and Dynamical Gauge Fields*, *New J. Phys.* **17**, 103021 (2015).
- [51] O. Dutta, L. Tagliacozzo, M. Lewenstein, and J. Zakrzewski, *Toolbox for Abelian Lattice Gauge Theories with Synthetic Matter*, *Phys. Rev. A* **95**, 053608 (2017).
- [52] L. Barbiero, C. Schweizer, M. Aidelsburger, E. Demler, N. Goldman, and F. Grusdt, *Coupling Ultracold Matter to Dynamical Gauge Fields in Optical Lattices: From Flux Attachment to 2 Lattice Gauge Theories*, *Sci. Adv.* **5**, 10 (2019).
- [53] E. Zohar, J. I. Cirac, and B. Reznik, *Quantum Simulations of Gauge Theories with Ultracold Atoms: Local Gauge Invariance from Angular-Momentum Conservation*, *Phys. Rev. A* **88**, 023617 (2013).
- [54] V. Kasper, F. Hebenstreit, F. Jendrzejewski, M. K. Oberthaler, and J. Berges, *Implementing Quantum Electrodynamics with Ultracold Atomic Systems*, *New J. Phys.* **19**, 023030 (2017).
- [55] D. González-Cuadra, E. Zohar, and J. I. Cirac, *Quantum Simulation of the Abelian-Higgs Lattice Gauge Theory with Ultracold Atoms*, *New J. Phys.* **19**, 063038 (2017).
- [56] G. Magnifico, D. Vodola, E. Ercolessi, S. P. Kumar, M. Müller, and A. Bermudez,  *$\mathbb{Z}_N$  Gauge Theories Coupled to Topological Fermions: QED<sub>2</sub> with a Quantum Mechanical  $\theta$  Angle*, *Phys. Rev. B* **100**, 115152 (2019).
- [57] C. Schweizer, F. Grusdt, M. Berngruber, L. Barbiero, E. Demler, N. Goldman, I. Bloch, and M. Aidelsburger, *Floquet Approach to  $\mathbb{Z}_2$  Lattice Gauge Theories with Ultracold Atoms in Optical Lattices*, *Nat. Phys.* **15**, 1168 (2019).
- [58] F. Görg, K. Sandholzer, J. Minguzzi, R. Desbuquois, M. Messer, and T. Esslinger, *Realization of Density-Dependent Peierls Phases to Engineer Quantized Gauge Fields Coupled to Ultracold Matter*, *Nat. Phys.* **15**, 1161 (2019).
- [59] A. Mil, T. V. Zache, A. Hegde, A. Xia, R. P. Bhatt, M. K. Oberthaler, P. Hauke, J. Berges, and F. Jendrzejewski, *A Scalable Realization of Local  $U(1)$  Gauge Invariance in Cold Atomic Mixtures*, *Science* **367**, 1128 (2020).
- [60] B. Yang, H. Sun, R. Ott, H.-Y. Wang, T. V. Zache, J. C. Halimeh, Z.-S. Yuan, P. Hauke, and J.-W. Pan, *Observation of Gauge Invariance in a 71-Site Quantum Simulator*, arXiv:2003.08945.
- [61] T. Senthil, *Symmetry-Protected Topological Phases of Quantum Matter*, *Annu. Rev. Condens. Matter Phys.* **6**, 299 (2015).
- [62] M. Creutz, *End States, Ladder Compounds, and Domain-Wall Fermions*, *Phys. Rev. Lett.* **83**, 2636 (1999).
- [63] C.-K. Chiu, J. C. Y. Teo, A. P. Schnyder, and S. Ryu, *Classification of topological quantum matter with symmetries*, *Rev. Mod. Phys.* **88**, 035005 (2016).
- [64] J. H. Kang, J. H. Han, and Y. Shin, *Realization of a Cross-Linked Chiral Ladder with Neutral Fermions in a 1D Optical Lattice by Orbital-Momentum Coupling*, *Phys. Rev. Lett.* **121**, 150403 (2018).
- [65] J. H. Kang, J. H. Han, and Y. Shin, *Creutz Ladder in a Resonantly Shaken 1D Optical Lattice*, *New J. Phys.* **22**, 013023 (2020).
- [66] J. Jünemann, A. Piga, S.-J. Ran, M. Lewenstein, M. Rizzi, and A. Bermudez, *Exploring Interacting Topological Insulators with Ultracold Atoms: The Synthetic Creutz-Hubbard Model*, *Phys. Rev. X* **7**, 031057 (2017).

- [67] A. Bermudez, E. Tirrito, M. Rizzi, M. Lewenstein, and S. Hands, *Gross-Neveu-Wilson Model and Correlated Symmetry-Protected Topological Phases*, *Ann. Phys. (N.Y.)* **399**, 149 (2018).
- [68] E. Tirrito, M. Rizzi, G. Sierra, M. Lewenstein, and A. Bermudez, *Renormalization Group Flows for Wilson-Hubbard Matter and the Topological Hamiltonian*, *Phys. Rev. B* **99**, 125106 (2019).
- [69] J. B. Kogut, *An Introduction to Lattice Gauge Theory and Spin Systems*, *Rev. Mod. Phys.* **51**, 659 (1979).
- [70] U. Borla, R. Verresen, F. Grusdt, and S. Moroz, *Confined Phases of One-Dimensional Spinless Fermions Coupled to  $Z_2$  Gauge Theory*, *Phys. Rev. Lett.* **124**, 120503 (2020).
- [71] U. Schollwck, *The Density-Matrix Renormalization Group in the Age of Matrix Product States*, *Ann. Phys. (N.Y.)* **326**, 96 (2011), Special Issue.
- [72] A. Kitaev and J. Preskill, *Topological Entanglement Entropy*, *Phys. Rev. Lett.* **96**, 110404 (2006).
- [73] M. Levin and X.-G. Wen, *Detecting Topological Order in a Ground State Wave Function*, *Phys. Rev. Lett.* **96**, 110405 (2006).
- [74] D. B. Kaplan, *A Method for Simulating Chiral Fermions on the Lattice*, *Phys. Lett. B* **288**, 342 (1992).
- [75] K. Jansen and M. Schmaltz, *Critical Momenta of Lattice Chiral Fermions*, *Phys. Lett. B* **296**, 374 (1992).
- [76] M. F. L. Golterman, K. Jansen, and D. B. Kaplan, *Chern-Simons Currents and Chiral Fermions on the Lattice*, *Phys. Lett. B* **301**, 219 (1993).
- [77] R. E. Peierls, *Quantum Theory of Solids*, International Series of Monographs on Physics (Clarendon Press, Oxford, 1955).
- [78] E. H. Lieb, *Flux Phase of the Half-Filled Band*, *Phys. Rev. Lett.* **73**, 2158 (1994).
- [79] X. G. Wen and A. Zee, *Winding Number, Family Index Theorem, and Electron Hopping in a Magnetic Field*, *Nucl. Phys.* **B316**, 641 (1989).
- [80] Y. Aharonov and D. Bohm, *Significance of Electromagnetic Potentials in the Quantum Theory*, *Phys. Rev.* **115**, 485 (1959).
- [81] Y. Kuno, T. Orito, and I. Ichinose, *Flat-Band Many-Body Localization and Ergodicity Breaking in the Creutz Ladder*, *New J. Phys.* **22**, 013032 (2020).
- [82] K. G. Wilson, *Quarks and Strings on a Lattice*, in *New Phenomena in Subnuclear Physics*, The Subnuclear Series Vol. 13 (Springer, Boston, MA, 1977), [https://doi.org/10.1007/978-1-4613-4208-3\\_6](https://doi.org/10.1007/978-1-4613-4208-3_6).
- [83] S. Ryu, A. P. Schnyder, A. Furusaki, and A. W. W. Ludwig, *Topological Insulators and Superconductors: Tenfold Way and Dimensional Hierarchy*, *New J. Phys.* **12**, 065010 (2010).
- [84] J. Zak, *Berry's Phase for Energy Bands in Solids*, *Phys. Rev. Lett.* **62**, 2747 (1989).
- [85] W. P. Su, J. R. Schrieffer, and A. J. Heeger, *Solitons in Polyacetylene*, *Phys. Rev. Lett.* **42**, 1698 (1979).
- [86] D. González-Cuadra, A. Dauphin, P. R. Grzybowski, P. Wójcik, M. Lewenstein, and A. Bermudez, *Symmetry-Breaking Topological Insulators in the  $Z_2$  Bose-Hubbard Model*, *Phys. Rev. B* **99**, 045139 (2019).
- [87] D. González-Cuadra, A. Bermudez, P. R. Grzybowski, M. Lewenstein, and A. Dauphin, *Intertwined Topological Phases Induced by Emergent Symmetry Protection*, *Nat. Commun.* **10**, 2694 (2019).
- [88] J. K. Asbóth, L. Oroszlány, and A. A. P. Pályi, *A Short Course on Topological Insulators: Band Structure and Edge States in One and Two Dimensions*, Lecture Notes in Physics (Springer, New York, 2016).
- [89] J. Hauschild and F. Pollmann, *Efficient Numerical Simulations with Tensor Networks: Tensor Network Python (TeNPy)*, *SciPost Phys. Lect. Notes* **5** (2018).
- [90] S. R. White, *Density Matrix Formulation for Quantum Renormalization Groups*, *Phys. Rev. Lett.* **69**, 2863 (1992).
- [91] R. Jackiw and C. Rebbi, *Solitons with Fermion Number 1/2*, *Phys. Rev. D* **13**, 3398 (1976).
- [92] D. K. Campbell and A. R. Bishop, *Solitons in Polyacetylene and Relativistic-Field-Theory Models*, *Phys. Rev. B* **24**, 4859 (1981).
- [93] M. V. Berry, *Quantal Phase Factors Accompanying Adiabatic Changes*, *Proc. R. Soc. A* **392**, 45 (1984).
- [94] Q. Niu and D. J. Thouless, *Quantised Adiabatic Charge Transport in the Presence of Substrate Disorder and Many-Body Interaction*, *J. Phys. A* **17**, 2453 (1984).
- [95] Q. Niu, D. J. Thouless, and Y.-S. Wu, *Quantized Hall Conductance as a Topological Invariant*, *Phys. Rev. B* **31**, 3372 (1985).
- [96] Y. Hatsugai, *Quantized Berry Phases as a Local Order Parameter of a Quantum Liquid*, *J. Phys. Soc. Jpn.* **75**, 123601 (2006).
- [97] T. Senthil and M. P. A. Fisher,  *$Z_2$  Gauge Theory of Electron Fractionalization in Strongly Correlated Systems*, *Phys. Rev. B* **62**, 7850 (2000).
- [98] T. Senthil and M. P. A. Fisher, *Fractionalization, Topological Order, and Cuprate Superconductivity*, *Phys. Rev. B* **63**, 134521 (2001).
- [99] Y. Zhang, T. Grover, A. Turner, M. Oshikawa, and A. Vishwanath, *Quasiparticle Statistics and Braiding from Ground-State Entanglement*, *Phys. Rev. B* **85**, 235151 (2012).
- [100] R. B. Laughlin, *Quantized Hall Conductivity in Two Dimensions*, *Phys. Rev. B* **23**, 5632 (1981).
- [101] E. J. Bergholtz and A. Karlhede, *Half-Filled Lowest Landau Level on a Thin Torus*, *Phys. Rev. Lett.* **94**, 026802 (2005).
- [102] F. Grusdt and M. Hönig, *Realization of Fractional Chern Insulators in the Thin-Torus Limit with Ultracold Bosons*, *Phys. Rev. A* **90**, 053623 (2014).
- [103] M. C. Strinati, E. Cornfeld, D. Rossini, S. Barbarino, M. Dalmonte, R. Fazio, E. Sela, and L. Mazza, *Laughlin-like States in Bosonic and Fermionic Atomic Synthetic Ladders*, *Phys. Rev. X* **7**, 021033 (2017).
- [104] N. Laflorencie, *Quantum Entanglement in Condensed Matter Systems*, *Phys. Rep.* **646**, 1 (2016).
- [105] L. Tagliacozzo, A. Celi, and M. Lewenstein, *Tensor Networks for Lattice Gauge Theories with Continuous Groups*, *Phys. Rev. X* **4**, 041024 (2014).
- [106] M. E. Fisher, *Statistical Mechanics of Dimers on a Plane Lattice*, *Phys. Rev.* **124**, 1664 (1961).
- [107] D. S. Rokhsar and S. A. Kivelson, *Superconductivity and the Quantum Hard-Core Dimer Gas*, *Phys. Rev. Lett.* **61**, 2376 (1988).



- [108] R. Moessner, S. L. Sondhi, and E. Fradkin, *Short-Ranged Resonating Valence Bond Physics, Quantum Dimer Models, and Ising Gauge Theories*, *Phys. Rev. B* **65**, 024504 (2001).
- [109] D. González-Cuadra, A. Dauphin, P. R. Grzybowski, M. Lewenstein, and A. Bermudez, *Dynamical Solitons and Boson Fractionalization in Cold-Atom Topological Insulators*, [arXiv:2003.10994](https://arxiv.org/abs/2003.10994).
- [110] D. González-Cuadra, A. Dauphin, P. R. Grzybowski, M. Lewenstein, and A. Bermudez,  *$\mathbb{Z}_n$  Solitons in Intertwined Topological Phases*, [arXiv:1908.02186](https://arxiv.org/abs/1908.02186).
- [111] R. Peierls, *The Size of a Dislocation*, *Proc. Phys. Soc.* **52**, 34 (1940).
- [112] F. R. N. Nabarro, *Dislocations in a Simple Cubic Lattice*, *Proc. Phys. Soc.* **59**, 256 (1947).